

Article

Spray Combustion Characteristics and Soot Emission Reduction of Hydrous Ethanol Diesel Emulsion Fuel Using Color-Ratio Pyrometry

Xiaoqing Zhang ^{1,2}, Tie Li ^{1,2,*}, Pengfei Ma ² and Bin Wang ^{1,2}

¹ Collaborative Innovation Centre for Advanced Ship and Deep-Sea Exploration, Shanghai Jiao Tong University, Shanghai 200240, China; zxq186@sjtu.edu.cn (X.Z.); wang_sjtu@163.com (B.W.)

² State Key Laboratory of Ocean Engineering, Shanghai Jiao Tong University, Shanghai 200240, China; mpfkumolj@163.com

* Correspondence: litie_sjtu@163.com; Tel.: +86-21-3420-8348

Received: 30 October 2017; Accepted: 28 November 2017; Published: 5 December 2017

Abstract: To elucidate the relationship between physicochemical properties, spray characteristics, and combustion performance, a series of experiments have been conducted in a constant volume vessel with injection of hydrous ethanol diesel emulsion and regular diesel. HE30 (emulsion with 30% volume fraction of 20% water-containing ethanol and 70% volume fraction of 0# diesel) is developed using Shah's technique and regular diesel is also employed for comparison. Firstly, the physicochemical properties of two kinds of fuels are investigated. Then, the non-evaporating and evaporating spray characteristics are examined through the high-speed shadowgraphs. Finally, spray combustion experiments under different ambient oxygen concentrations are carried out, and color-ratio pyrometry (CRP) is applied to measure the flame temperature and soot concentration (*KL*) distributions. The results indicate that the physicochemical properties, such as density, surface tension, kinematic viscosity, cetane number, and oxygen content, have significant impact on the spray mixture formation and combustion performance. HE30 exhibits lower soot emissions than that of regular diesel. Further analysis supports the standpoint that the hydrous ethanol diesel emulsion can suppress the soot and NO_x simultaneously. Therefore, the hydrous ethanol diesel emulsion has great potential to be an alternative clean energy resource.

Keywords: bioethanol; hydrous ethanol diesel emulsions; physicochemical property; spray combustion; soot emission

1. Introduction

The attention to environmental pollution problems has resulted in stringent emission regulations worldwide. The utilization of clean fuel is becoming both urgent and globally attractive. Biomass energy is considered an alternative energy resource of traditional fossil fuels [1–5]. Many studies focused on the development and application of biomass energy. These literatures [6–11] investigated the performance and emission of a diesel engine fuelled with biomass fuels and its blends. Their results show that biomass fuels could be a potential fuel for diesel engines. Bioethanol, as a carbon neutral and renewable source of energy, has also attracted significant attention [7,12,13]. However, high energy consumption is required for the bioethanol production process. Shapouri et al. [14] pointed out that the energy consumption accounts for up to 37% in the total input energy in the case of the ethanol production with corn as feedstock. Richard et al. [15] pointed out that adding water to ethanol further increases injected fuel volume, but the increase in combustion duration and reduction in combustion stability are not significant with up to 30% water by volume.

Martinez-Frias et al. [16] found that the use of hydrous ethanol instead of high purity ethanol can improve the balance between energy gain and energy expenditure for bioethanol production. Meanwhile, the high hydrophilicity of ethanol will lead to stratification when hydrous ethanol diesel blends are used. Surfactants are added into the blends to form emulsions and achieve stability [17,18].

The utilization of hydrous ethanol instead of pure ethanol can improve the overall energy balance and production cost of bioethanol. Consequently, more studies have been focused on the combustion of hydrous ethanol in recent years. Costa and Sodré [19] compared the performance and emissions from a production spark-ignited (SI) engine with the hydrous ethanol–diesel–ethanol blends. The results indicate that the use of hydrous ethanol leads to higher power and thermal efficiency. Breaux and Acharya [20] carried out an experimental study in a swirl-stabilized combustor for a gas turbine by using the hydrous ethanol with various volume fraction of water. Ambrós et al. [21] pointed out that hydrous ethanol is more efficient than pure ethanol by experimentally investigating the effects of hydrous ethanol with various water contents in volume in a SI engine. Morsy [22] investigated a direct injection diesel engine fumigated with hydrous ethanol. Datta and Mandal [13] has found that it can improving the NO_x emission with diesel–ethanol blend compared to diesel–methanol blend. Li et al. [23] carried out a profound investigation on the characteristics of non-evaporating, evaporating, and burning sprays under various injection and ambient conditions in a high-temperature, high-pressure, constant-volume combustion vessel.

As its component of hydroxyl (OH), hydrous ethanol diesel blends can reduce the soot emission in a diesel engine [24,25]. However, there is trade-off relation between NO_x and soot formation for combustion of a diesel engine [26,27]. These literatures have focused on the low-temperature combustion (LTC) [8,28–31]. The results support the view that LTC has the potential to reduce soot and NO_x emission simultaneously. However, there are still controversial discussions on this issue.

As discussed previously, the two-colour method has been developed and used to measure the soot temperature and concentration of diesel since the 1940s [32–35]. However, it has a high uncertainty during using the method [36]. Meanwhile, the colour-ratio pyrometry (CRP) method, using the three-colour ratio, can provide two independent measures for determining the temperature and soot concentration (*KL*) [37]. In the development of the imaging technique, high-speed CMOS camera (NAC HX-6, NAC image technology Inc., Tokyo, Japan) was applied in CRP, where the red, green, and blue channels detect the light simultaneously.

The above literatures indicate that hydrous ethanol, as an addition into diesel fuel, can decrease pollution emissions, while the hydrous ethanol diesel emulsions can be used for energy optimization. However, little research has been conducted on a full investigation of this issue, especially focusing on the mechanism of soot reduction. Moreover, further investigation is needed to identify the role of hydrous ethanol diesel. In this paper, a comprehensive experiment has been carried out in a constant volume to examine the spray combustion performances of hydrous ethanol diesel emulsions and diesel fuel. The physicochemical properties and spray characteristics are obtained. The flame temperature and *KL* are measured by using the CRP method.

2. Experiments and Methodology

2.1. Development of Emulsions

The emulsions HE30 were developed by employing the Shah's technique [38]. The detailed procedure can be found in the literature [23]. The density of HE30 was determined by measuring the volume and weight of the samples. Surface tension was measured with the surface tension meter (BZY-201, Shanghai Fangrui instrument Co., Ltd., Shanghai, China) based on the national standard GB/T6541-86. Kinematic viscosity was measured by the rotary viscometer (NDJ-8S, Shanghai precision instrument Co., Ltd., Shanghai, China). Distillation temperature can be obtained by the distillation tester (DLYS-101A, Dalian Yushuo technology development Co., Ltd., Dalian, China) based on the standard GB/T6536-2010. Cetane number, lower heating value, and oxygen content of the fuels

were estimated with the mass fractions of the components in the emulsions. The instruments with uncertainty and range are listed in Table 1.

Table 1. Instruments with their range, accuracy and uncertainty analysis.

No.	Instruments	Measuring Range	Accuracy	Percentage Uncertainties
1	BZY-201	0~400 mN/m	0.01 mN/m	0.04
2	DLYS-101A	-2~+400 °C	±0.5 °C	0.125
3	NDJ-8S	10~200 × 10 ⁴ (m ²)/s	±1.0%	0.50

2.2. Experimental Setups for Spray Combustion

Figure 1 shows the schematic of the experimental system for characterization of spray combustion processes. The spray combustion experiments are implemented on this platform system. In this study, the high-speed shadowgraph is employed to film the two-phase sprays under both non-evaporation and evaporation conditions [23]. The high-speed CMOS camera (NAC HX-6, NAC image technology Inc., Tokyo, Japan) and the xenon lamp were used to establish the optical system of shadowgraph. The frame rate and exposure time of the camera were set as 50,000 fps and 1.1 μs, respectively. More detail information can be seen in Table 2. For flame temperature and *KL* measurements, the CRP method is employed, and the optical schematic is established in Figure 2. The parameter details for the injection system and experimental conditions are listed in Table 2. Five shots were repeated for each experimental condition in this study.

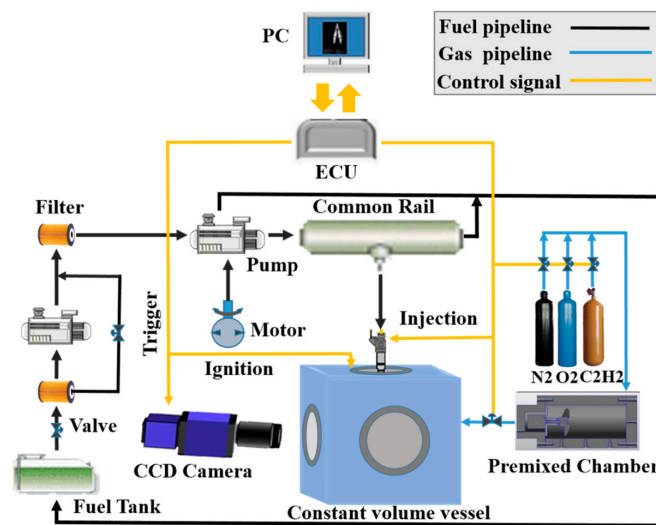


Figure 1. Schematic of the experimental system for spray combustion.

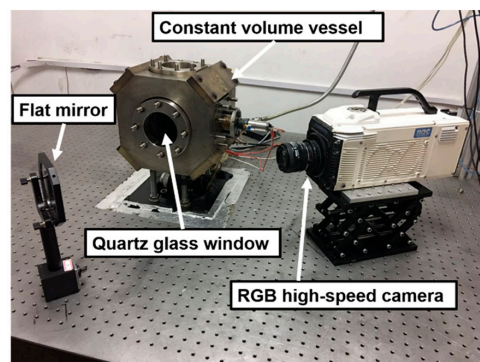


Figure 2. Optical system schematic for the color-ratio pyrometry (CRP) method.

Table 2. Specifications for the injection system and experimental conditions.

Experimental Conditions	Spray	Combustion
Injector type	Mini sac	Mini sac
Orifice diameter (mm)	0.28	0.28
Ambient density (kg/m ³)	15	15
Ambient temperature (K)	900/293 ¹	900
Injection pressure (MPa)	120	120
Injection duration (ms)	2.2	2.2
Imaging speed (fps)	50,000	25,000
Exposure time (μs)	1.1	1.1/3 ²
F-number	2.8	2.8/5.6 ²

¹ The ambient temperature for non-evaporating spray is 293 K while the temperature of the evaporating spray is 900 K; ² The exposure time and F-number parameters of the camera for high ambient O₂ concentrations (21%) and low ambient O₂ concentrations (12%) are set as 1.1 μs and F-2.8 and 3.3 μs and F-5.6, respectively.

2.3. CRP Theory

The CRP method measures the intensity of the luminous flux from the hot, incandescent soot in the flame, which is behaving as a black body emitter. Matsui et al. [35] pointed out that the temperature of the ambient gas changes with time the radiation can be ignored, since it is small compared to the heat conductivity. Therefore, the temperature of the soot can approximately represent that of spray flame. The basic principle of the color ratio method is the heat radiation theory, and Hottel and Broughton empirical formula. By calculating the radiation intensity ratio of the soot through the different channels of red, green and blue, the flame temperature, and soot concentration are obtained. For absolute black bodies, their radiation intensity is expressed by Equation (1):

$$I_b(\lambda, T) = \frac{C_1}{\lambda^5(\exp(C_2/\lambda T) - 1)} \quad (1)$$

where C_1 and C_2 are the Planck constant, and λ is the corresponding wavelength.

For the hot smoke in the flame, the radiation intensity can be calculated by Equation (2):

$$I_s(\lambda, T) = \varepsilon_\lambda I_b(\lambda, T) = \varepsilon_\lambda \frac{C_1}{\lambda^5(\exp(C_2/\lambda T) - 1)} \quad (2)$$

Another basic principle of the color ratio method is the Hottel and Broughton empirical formula as shown in Equation (3):

$$\varepsilon_\lambda = 1 - e^{(-KL/\lambda^\alpha)} \quad (3)$$

where KL is a characterization parameter of soot density and α is 1.38 or 1.39 in the visible range [32].

For the red channel, for example, the absolute radiation intensity of the hot smoke can be expressed as Equation (4):

$$I_{s,R}(T) = \int_{\lambda_1}^{\lambda_2} f_R(\lambda) \varepsilon_\lambda I_b(\lambda, T) d\lambda \quad (4)$$

Then, two ratio equations can be obtained as Equation (5):

$$\begin{cases} \frac{R}{G} = \frac{a_R \int_{\lambda_1}^{\lambda_2} f_R(\lambda) (1 - e^{-KL/\lambda^\alpha}) \frac{C_1}{\lambda^5(\exp(C_2/\lambda T) - 1)} d\lambda + b_R}{a_G \int_{\lambda_1}^{\lambda_2} f_G(\lambda) (1 - e^{-KL/\lambda^\alpha}) \frac{C_1}{\lambda^5(\exp(C_2/\lambda T) - 1)} d\lambda + b_G} \\ \frac{R}{B} = \frac{a_R \int_{\lambda_1}^{\lambda_2} f_R(\lambda) (1 - e^{-KL/\lambda^\alpha}) \frac{C_1}{\lambda^5(\exp(C_2/\lambda T) - 1)} d\lambda + b_R}{a_B \int_{\lambda_1}^{\lambda_2} f_B(\lambda) (1 - e^{-KL/\lambda^\alpha}) \frac{C_1}{\lambda^5(\exp(C_2/\lambda T) - 1)} d\lambda + b_B} \end{cases} \quad (5)$$

Equation (5) is a transcendental equation, where the look-up table method is used and the judgement error parameter E can be given as Equation (6):

$$E = (R/G - \alpha_{i,j})^2 + (R/B - \beta_{i,j})^2 \quad (6)$$

where R , G and B are the brightness values (RGB) of the red, green and blue channels of a point in the flame image. $\alpha_{i,j}$ and $\beta_{i,j}$ are the ratio of R/G and ratio of R/B at the i row and the j column in the table, respectively [37].

In this study, the linear relationship between RGB value and light intensity was checked before the test, the calibration for red, green and blue channels and apparent temperatures at various setting parameters of the camera have been conducted in the experiment. The neutral filter was used in the optical setups for some experimental conditions. These details can be referred to the literature [36]. The uncertainties may be caused by parameters setting, calibration and quartz windows etc. More detailed analysis can also be seen in the literature [36].

3. Results and Discussion

3.1. Physicochemical Properties

Table 3 shows the physicochemical properties of HE30 and diesel fuel. The density of HE30 is heavier than that of diesel fuel because hydrous ethanol is greater than diesel fuel. The surface tensions of HE30 are less than that of diesel fuel given that it is mixed results of different components with various surface tensions. The kinematic viscosity at 20 °C of HE30 is a little higher than that of diesel fuel. While the latent heat of evaporation for HE30 is apparently higher than that of diesel fuel, it is easily explained that the latent heat of water and ethanol is higher than that of diesel fuel. Meanwhile, HE30 has a lower cetane number and heating value compared to diesel.

Table 3. Physicochemical properties of diesel and HE30.

Physicochemical Properties	Diesel	HE30
Stable time (h)	-	103
Mass fraction of hydrous ethanol (%)	0	28.3
Density (kg/m ³)	818	831
Surface tension (mN/m)	28.5	28.4
Kinematic viscosity @ 20 °C (mm ² /s)	3.35	4.02
Latent heat of vaporization (kJ/kg)	270	535
Cetane number	50	36
Lower heating value (MJ/kg)	42.8	36.3
Oxygen content (mass %)	0	14.4

Physicochemical properties play an important role in mixture formation, ignition, and combustion processes of the diesel fuel. The density, kinematic viscosity, and surface have significant influence on the velocity and momentum of spray droplets, and affect the liquid breakup and spray formation. Therefore, these parameters can be used for spray characteristics analysis. Meanwhile, the latent heat of evaporation, cetane number, lower heating value, and oxygen content affect the mixture formation, ignition, and combustion processes [39]. The latent heat of evaporation can affect the flame temperature, the greater latent heat of evaporation of fuels will cost more energy for evaporation rather than the temperature increase in the combustion. The cetane number is an important index to determine the ignition delay (ID).

3.2. Characteristics of Non-Evaporating and Evaporating Sprays

Figure 3 exhibits the temporal developments of the non-evaporating sprays (a) and evaporating sprays (b) for the diesel and HE30 by using high-speed shadowgraph, respectively. Each experimental

condition repeated 5 shots, the fluctuation of each shot is relative small. The spray tip penetration and cone angle for both non-evaporating and evaporating conditions are demonstrated in Figure 4. For both spray conditions, HE30 exhibits a higher penetration rate and a narrower cone angle than that of the diesel, and it is more obvious for the non-evaporating sprays. Both spray tip penetration and cone angle are dependent on energy and momentum. For the non-evaporating spray, HE30 has a greater momentum given its higher density compared to diesel. However, in the evaporating condition, the fuel at the boundary is in the vapour phase. Therefore, the penetration rate is more dependent on the evaporation rate. During a short period after start of injection (SOI), there is a sharp rise for the spray cone angle, before proceeding to quasi-steady state. During this initial transient, liquid is accelerated through the nozzle and enters the gas volume surrounding the nozzle. The spray angles of HE30 under evaporating and non-evaporating have larger variability, it is the result of the evaporation of HE30.

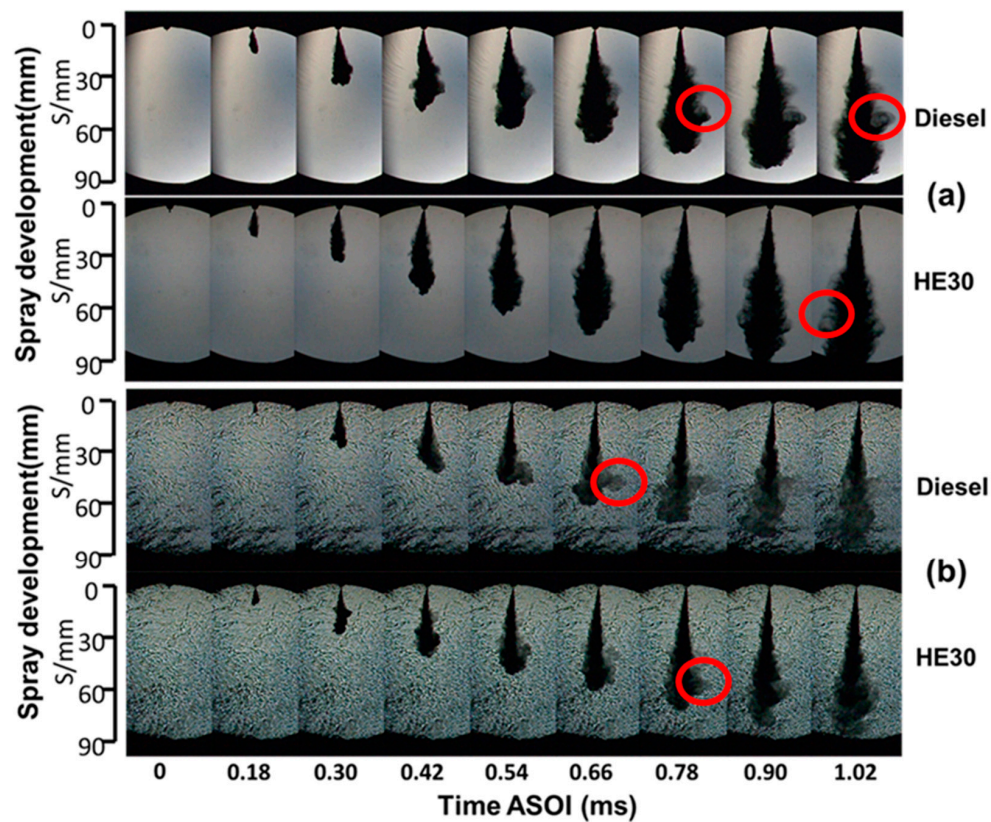


Figure 3. Temporal development of non-evaporating (a) and evaporating (b) sprays by using high-speed shadowgraph. ($P_{inj} = 120$ MPa, $P_a = 4.0$ MPa, $\rho_a = 15$ kg/m³, $T_a = 293$ K (a); $T_a = 900$ K (b); Frame rate: 50,000 fps, Exposure time: 1.1 μ s).

Furthermore, many vortex clusters can be seen at the edge of the spray (see red circles in the Figure 3). These vortex structures are generated by the interaction between sprays and surrounding air during the injection with a high pressure, and they play an important role in the fuel-air mixing. For evaporating sprays, these deformation sprays are considered to support the occurrence of micro-explosion in the sprays. However, these vortex structures also can be found in the sprays of regular diesel in this study, which seems not to backup this viewpoint.

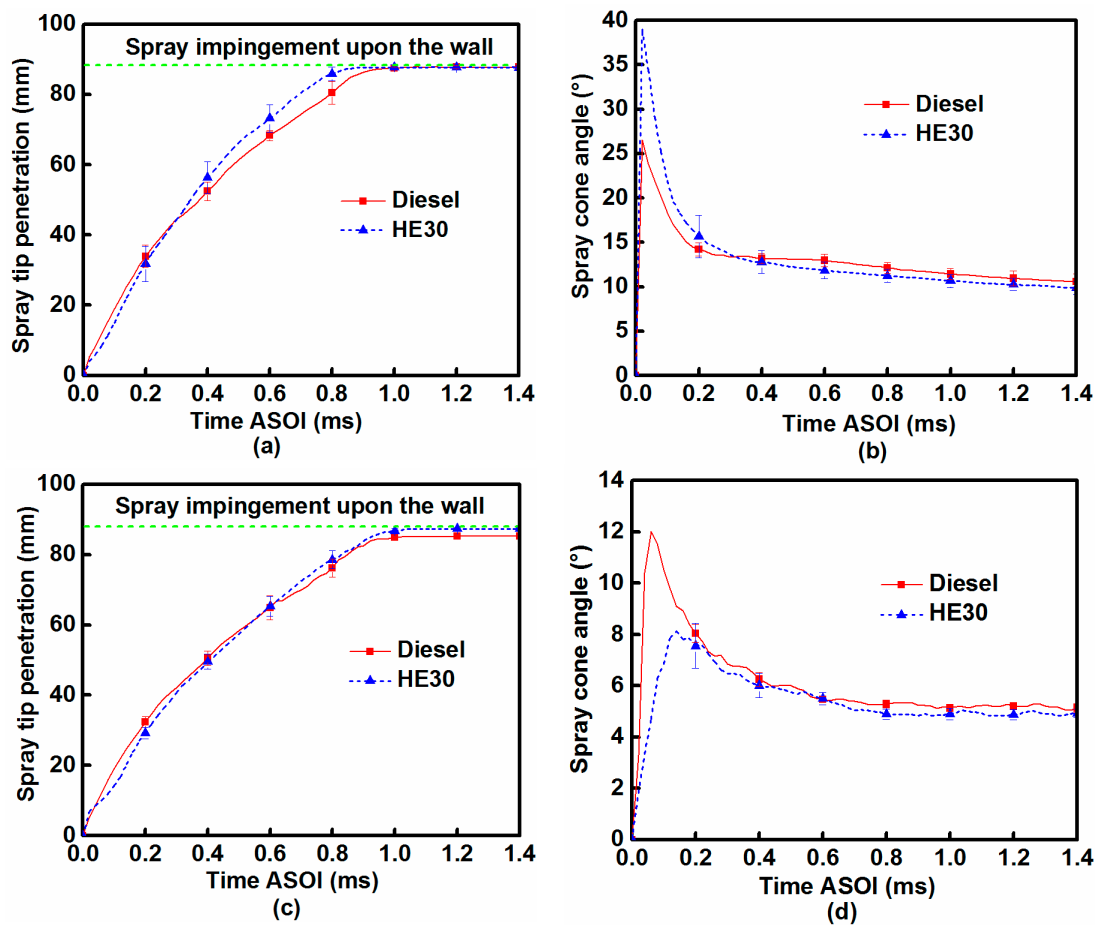


Figure 4. Spray tip penetrations and the cone angle of diesel and HE30. (a) Spray tip penetration for non-evaporation; (b) Spray cone angle for non-evaporation; (c) Spray tip penetration for evaporation; and (d) Spray cone angle for evaporation.

Moreover, as illustrated in Figure 4a,c, the penetration rate of the sprays for all the fuels are fast during initial period as the momentum generated by high speed injection. It slightly decreased as the resistance of ambient air and evaporation of fuels. The spray of HE30 impinged upon the wall earlier as it penetrated slightly faster than regular diesel. The wall impingement increase the HC, CO and NO_x emissions of a diesel engine [40,41]. Therefore, the hydrous ethanol diesel emulsion, such as HE30, increases the chance of wall impingement, which is an issue to be considered for diesel engines burning the bio-ethanol fuels.

3.3. Characteristics of Combustion

3.3.1. Spatially Resolved Results of Temperature and KL

Figure 5 shows the flame temperature and KL factor distributions at the developing stage under different ambient O₂ concentrations. The diesel fuel and HE30 have a similar spray length as the evaporating penetrations for two fuels are very similar. However, with a close observation, HE30 shows a little longer penetration distance. HE30 shows a narrow soot areas compared to regular diesel, which is coincident with the result in the literature [34]. It could be caused by the different oxygen component in two fuels, and regular diesel needs penetrate longer in the longitudinal direction to be ignited [42]. On the other hand, the high KL factors appear at the tip and heart part of the flame, while the low KL factors mainly stack up at the end part of the flame. This is due to the local ambient O₂ concentration in inner flame is lower than that of the external region.

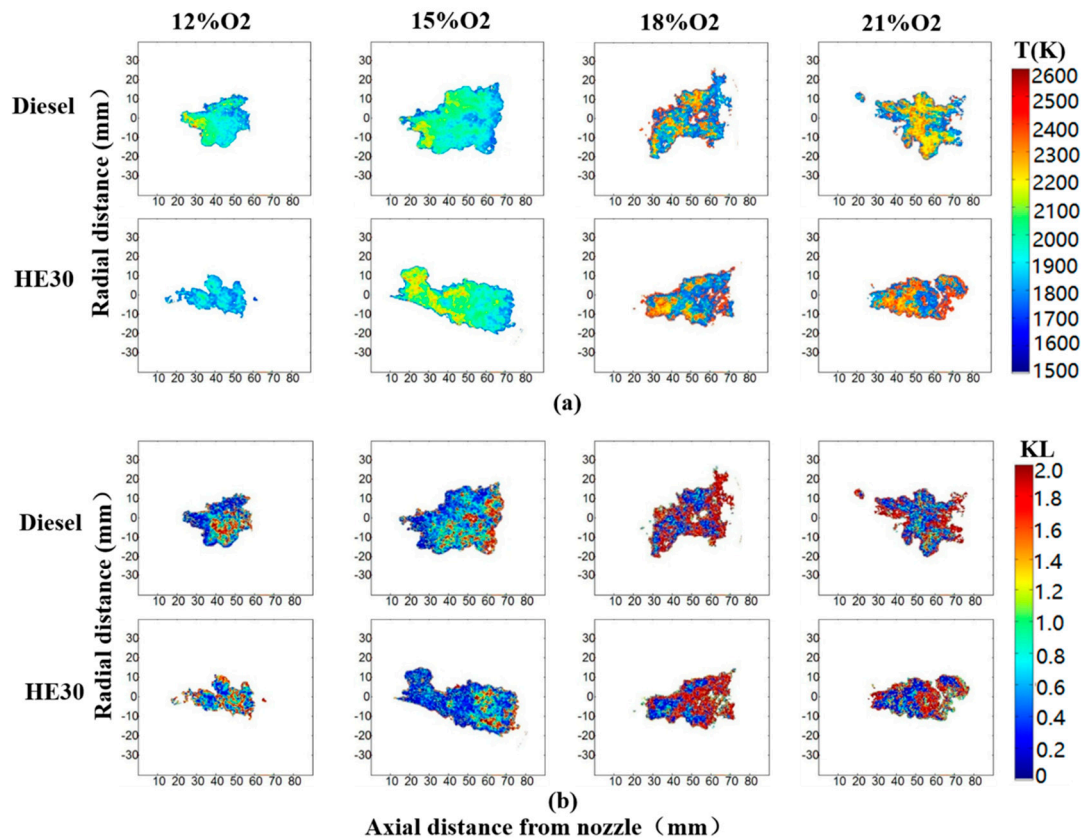


Figure 5. Flame temperature and KL distributions of various fuels at the developing stage for 12%, 15%, 18% and 21% ambient O_2 concentrations, (a) flame temperature and (b) KL .

3.3.2. Flame Temperature

The KL and flame temperature of diesel and HE30 sprays are measured. The temporally resolved flame temperature of the diesel fuel and HE30 under 21% ambient O_2 concentration and 12% ambient O_2 concentration are presented in Figure 6. The average temperature at a certain moment was calculated by cloud charts obtained from the high-speed camera (see Figure 5). For each chart at a certain moment, the average temperature was calculated as the arithmetic mean value of all pixel points in the chart. Three stages of combustion processes can be observed, namely, the temperature increases quickly at the developing stage, maintains a relevant steady at quasi-steady state and decreases quickly at the end of the SOI. HE30 exhibits a higher flame temperature at 12% ambient O_2 concentration than that of diesel fuel. However, it is not clear at 21% O_2 concentration. It may be explained that both the ambient O_2 concentration and the type of fuels affect the combustion behavior and the temperature of flame. However, the effect of ambient O_2 concentration is prominent under the 21% ambient O_2 concentration. High temperature can promote the NO_x formation, and HE30 can suppress it to some extent.

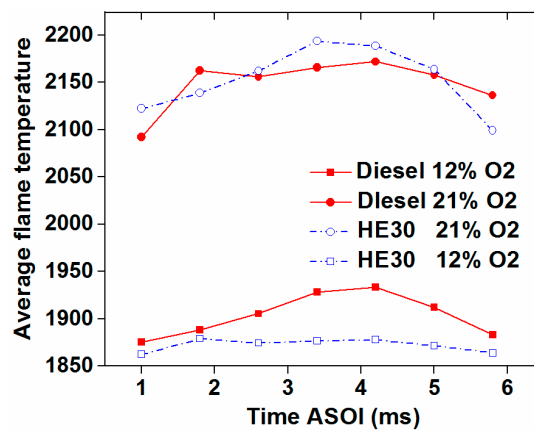


Figure 6. Temporally resolved average flame temperature of diesel and HE30 under 21% ambient O₂ concentration and 12% ambient O₂ concentration.

3.3.3. KL Factor Distributions

Figure 7 shows the proportions of various KL factors after the SOI for diesel fuels and HE30. The initial time is selected at 1.0 ms due to various ID of the diesel fuel and HE30. The value of KL represents the soot concentration [35], the larger value of the KL means the greater soot formation at that moment. The average value of KL at a certain moment can be obtained as the similar means used in calculating the average temperature. However, as the KL distributions are listed statistically at a certain moment, the average value of KL is decided by the proportion of large-value KL commonly. For the same fuel, such as HE30, the proportion of large-value of KL ($KL > 1.6$) under the 12% ambient O₂ concentration is obvious higher than that under the 21% ambient O₂ concentration at the end of combustion (5.8 ms), while it is not clear at the beginning of the SOI. This is the result of oxidation of soot, a further discussion will be made in this study. The diesel shows the similar trend. While for the same ambient O₂ concentration, such as 21% ambient O₂ concentration, the proportion of large-value of KL for HE30 is obvious lower than that of the diesel in the whole combustion process. It also has the similar trend under the 12% ambient O₂ concentration.

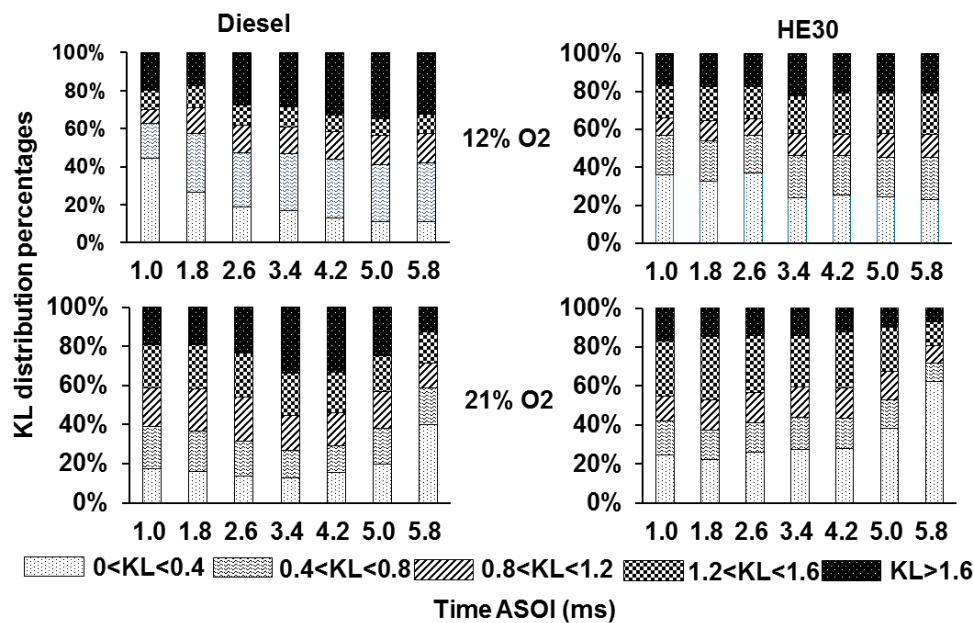


Figure 7. Time resolved KL factor distributions for HE30 (right) and diesel (left) at 12% ambient O₂ concentration and 21% ambient O₂ concentration.

The temporally resolved soot distributions can be divided into two processes, namely, soot formation process, and soot oxidation process. For soot formation process, the local equivalence ratio is a significant factor given that the soot precursors are generated in the fuel-rich premixed burn region [43,44]. For the soot oxidation process, López et al. [45] pointed out that the mixing capability and bulk temperature are the main impact factors, and a parameter is defined to explain the mixing capability. As seen in Figure 7, for the same fuel, an obviously lower percentage of large-value KL are demonstrated under 21% ambient O_2 concentration at the end stage of combustion, while there is not clear difference between two ambient O_2 concentrations at the beginning stage of combustion. This result indicates that the higher ambient O_2 concentration and the high temperature are favour to the oxidation of soot, conversely, the oxidation of soot is suppressed under low ambient O_2 concentration and low temperature. Regarding with the result at the beginning of the combustion, it can be explained by two reasons. One is the effect of the different ignition delay (ID) of two fuels. As the same coordinate origin of the time axis is used, so the different stage of combustion for two fuels are developing at one moment after SOI, which may affect the KL formation at the initial period of combustion. The other is the effect of overexposure of the camera. The luminance of the flame under 21% ambient O_2 concentration is very bright, it may cause the overexposure of some area in flame, which also affects the calculation results. As seen in Figure 5, some areas become deep red as overexposure under 21% ambient O_2 concentration. Therefore, a lower value of KL can't be seen under the 21% ambient O_2 concentration at the initial stage period of combustion. Meanwhile, for the same ambient oxygen concentration, a relevant greater percentage of low-value KL factors are presented under 12% ambient O_2 concentration because the hydrous ethanol diesel emulsion HE30 has a better mixing capability than that of the diesel fuel.

Further discussion regarding the mixing capability of HE30 and the diesel fuel. As mentioned above, HE30 has a smaller cetane number compared to the diesel fuel; therefore, HE30 has a longer ID in the spray combustion process, which implies a longer time for HE30 mixing with air when burning. On the other hand, as discussed above, HE30 has a slightly higher spray tip penetration than the diesel fuel, especially a longer maximum liquid phase length [23], it is beneficial for air entrainment and promotes the fuel-air mixing. For the soot oxidation process, the major factors are the flame temperature and ambient oxygen concentration. In this study, the soot oxidation is seriously restrained by the low ambient oxygen concentration of 12% (see Figure 7). The low ambient oxygen concentration always goes along with the low flame temperature, which are both disadvantageous for soot oxidation.

Moreover, from the chemical kinetic point of view, the component of hydroxyl (OH) exists in HE30. It can promote the hydrocarbon molecules oxidized to CO_2 , besides, it is also beneficial on the oxidation of soot, thus it can reduce the soot emissions. As discussed above, HE30 should have a low flame temperature than that of the diesel fuel when burning given the existence of wet ethanol. Even though it is not very notable here (see Figure 6), it did not prevent us from drawing a conclusion. Therefore, this study supports the viewpoint that hydrous ethanol diesel emulsions can suppress the soot production.

4. Conclusions

HE30, as a representative of hydrous ethanol diesel emulsions, and diesel fuel, as a comparison, are selected for investigation. A series of experiments have been carried out to investigate the physicochemical properties, characteristics of non-evaporating and evaporating sprays, as well as the combustion performance and soot production of HE30, and diesel fuel. The major findings are summarized as follows.

- (1) Hydrous ethanol diesel emulsions have slightly higher density and kinematic viscosity with lower surface tension, cetane number, and heating value. These properties have significant influence on the formation of spray mixtures. The longer ID of emulsions resulted in more abundant mixture, which can improve the combustion and reduce the soot production.

- (2) Similarly, the spray cone angle and tip penetration length are also affected by the physicochemical properties. Hydrous ethanol diesel emulsions show a slightly higher penetration rate and smaller cone angle. Therefore, a smaller soot formation area is obtained and more air can be rolled inside the spray, which can improve the combustion and reduce the soot production.
- (3) The comparative analysis of the *KL* factors distribution and flame temperature shows that hydrous ethanol diesel emulsions exhibit a lower soot production as well as a relevant lower flame temperature under the same ambient conditions. This result supports the standpoint that hydrous ethanol diesel emulsions can suppress the NO_x and soot emissions simultaneously.
- (4) Ambient O₂ concentration is a significant factor in combustion characteristics of hydrous ethanol diesel emulsions and diesel fuel. The flame temperature and ambient O₂ concentration affect the soot oxidation process. High flame temperature and high ambient O₂ concentration are favourable for soot oxidation, conversely, low flame temperature and low ambient O₂ concentration are disadvantageous for soot oxidation.
- (5) Therefore, hydrous ethanol diesel emulsions could potentially become an alternative clean fuel to fossil fuels in the future, although many challenges would still need to be resolved.

Acknowledgments: The financial supports by the Natural Science Foundation of China (91541104) and “ChenXing” project of Shanghai Jiao Tong University (AF0100071) is gratefully acknowledged. The contributions by the former graduate students, Tao Guo is highly appreciated.

Author Contributions: This is to confirm that all the authors have contributed in diverse ways at all stages of the research including research design, data collection and final preparation of the manuscript. All authors have read and approved the final manuscript.

Conflicts of Interest: The authors declare no potential conflict of interest.

Nomenclature

HE30	hydrous ethanol diesel emulsion with the 30% fraction of hydrous ethanol
CRP	colour-ratio pyrometry
NO _x	nitrogen oxides
SI	spark ignition
OH	hydroxyl
LTC	low temperature combustion
<i>KL</i>	soot concentration
CMOS	complementary metal oxide semiconductor
RGB	red, green and blue channels of high speed camera
C_1	Plank’s first constant
C_2	Plank’s second constant
ε_λ	monochromatic emissivity
ID	ignition delay
SOI	start of ignition
ASOI	after start of ignition
P_a	ambient pressure
P_{inj}	injection pressure
T_a	ambient temperature
ρ_a	density of ambient gas, (kg/m ³)

References

1. Ghadikolaei, M.A. Effect of alcohol blend and fumigation on regulated and unregulated emissions of IC engines—A review. *Renew. Sustain. Energy Rev.* **2016**, *57*, 1440–1495. [[CrossRef](#)]
2. Algayyim, S.J.M.; Wandel, A.P.; Yusaf, T.; Hamawand, I. Production and application of ABE as a biofuel. *Renew. Sustain. Energy Rev.* **2018**, *82*, 1195–1214. [[CrossRef](#)]

3. Hoekman, S.K.; Broch, A.; Liu, V. Environmental Implications of Higher Ethanol Production and Use in the US.: A literature review. Part I—Impacts on water, soil, and air quality. *Renew. Sustain. Energy Rev.* **2018**, *81*, 3140–3158. [[CrossRef](#)]
4. Rahman, M.; Rasul, M.; Hassan, N.; Hyde, J. Prospects of Biodiesel Production from Macadamia Oil as an Alternative Fuel for Diesel Engines. *Energies* **2016**, *9*, 403. [[CrossRef](#)]
5. Giakoumis, E.G.; Rakopoulos, D.C.; Rakopoulos, C.D. Combustion noise radiation during dynamic diesel engine operation including effects of various biofuel blends: A review. *Renew. Sustain. Energy Rev.* **2016**, *54*, 1099–1113. [[CrossRef](#)]
6. Chauhan, B.S.; Kumar, N.; Cho, H.M.; Lim, H.C. A study on the performance and emission of a diesel engine fueled with Karanja biodiesel and its blends. *Energy* **2013**, *56*, 1–7. [[CrossRef](#)]
7. El-Faroug, M.; Yan, F.; Luo, M.; Fiifi Turkson, R. Spark Ignition Engine Combustion, Performance and Emission Products from Hydrous Ethanol and Its Blends with Gasoline. *Energies* **2016**, *9*, 984. [[CrossRef](#)]
8. Wang, Z.; Wu, S.; Huang, Y.; Chen, Y.; Shi, S.; Cheng, X.; Huang, R. Evaporation and Ignition Characteristics of Water Emulsified Diesel under Conventional and Low Temperature Combustion Conditions. *Energies* **2017**, *10*, 1109. [[CrossRef](#)]
9. Lee, S.; Lee, C.S.; Park, S.; Gupta, J.G.; Maurya, R.K.; Agarwal, A.K. Spray characteristics, engine performance and emissions analysis for Karanja biodiesel and its blends. *Energy* **2017**, *119*, 138–151. [[CrossRef](#)]
10. Rakopoulos, D.C.; Rakopoulos, C.D.; Giakoumis, E.G.; Komninos, N.P.; Kosmadakis, G.M.; Papagiannakis, R.G. Comparative evaluation of ethanol, n-butanol, and diethyl ether effects as biofuel supplements on combustion characteristics, cyclic variations, and emissions balance in light-duty diesel engine. *J. Energy Eng.* **2016**, *143*, 04016044. [[CrossRef](#)]
11. Algayyim, S.J.M.; Wandel, A.P.; Yusaf, T.; Hamawand, I. The impact of n-butanol and iso-butanol as components of butanol-acetone (BA) mixture-diesel blend on spray, combustion characteristics, engine performance and emission in direct injection diesel engine. *Energy* **2017**, *140*, 1074–1086. [[CrossRef](#)]
12. Kumar, B.R.; Saravanan, S. Use of higher alcohol biofuels in diesel engines: A review. *Renew. Sustain. Energy Rev.* **2016**, *60*, 84–115. [[CrossRef](#)]
13. Datta, A.; Mandal, B.K. Impact of alcohol addition to diesel on the performance combustion and emissions of a compression ignition engine. *Appl. Therm. Eng.* **2016**, *98*, 670–682. [[CrossRef](#)]
14. Shapouri, H.; Duffield, J.; Wang, M. The energy balance of corn ethanol revisited. *Trans. Am. Soc. Agric. Eng.* **2003**, *46*, 959–968. [[CrossRef](#)]
15. Stone, R.; Chen, L.; Hinton, N.; Leach, F.; Xu, F. GDI engine operation with ethanol/gasoline blends and aqueous ethanol. *J. Autom. Saf. Energy* **2012**, *3*, 257–264.
16. Martinez-Frias, J.; Aceves, S.M.; Flowers, D.L. Improving ethanol life cycle energy efficiency by direct utilization of wet ethanol in HCCI engines. *J. Energy Resour. Technol.* **2007**, *129*, 332–337. [[CrossRef](#)]
17. Campos-Fernández, J.; Arnal, J.M.; Gómez, J.; Dorado, M.P. A comparison of performance of higher alcohols/diesel fuel blends in a diesel engine. *Appl. Energy* **2012**, *95*, 267–275. [[CrossRef](#)]
18. Guo, Z.; Wang, S.; Wang, X. Stability mechanism investigation of emulsion fuels from biomass pyrolysis oil and diesel. *Energy* **2014**, *66*, 250–255. [[CrossRef](#)]
19. Costa, R.C.; Sodr e, J.R. Hydrous ethanol vs. gasoline-ethanol blend: Engine performance and emissions. *Fuel* **2010**, *89*, 287–293. [[CrossRef](#)]
20. Breaux, B.B.; Acharya, S. The effect of elevated water content on swirl-stabilized ethanol/air flames. *Fuel* **2013**, *105*, 90–102. [[CrossRef](#)]
21. Ambr os, W.; Lanzanova, T.; Fagundez, J.; Sari, R.; Pinheiro, D.; Martins, M.; Salau, N. Experimental analysis and modeling of internal combustion engine operating with wet ethanol. *Fuel* **2015**, *158*, 270–278. [[CrossRef](#)]
22. Morsy, M.H. Assessment of a direct injection diesel engine fumigated with ethanol/water mixtures. *Energy Convers. Manag.* **2015**, *94*, 406–414. [[CrossRef](#)]
23. Li, T.; Zhang, X.-Q.; Wang, B.; Guo, T.; Shi, Q.; Zheng, M. Characteristics of non-evaporating, evaporating and burning sprays of hydrous ethanol diesel emulsified fuels. *Fuel* **2017**, *191*, 251–265. [[CrossRef](#)]
24. Lapuerta, M.; Garcia-Contreras, R.; Campos-Fern andez, J.; Dorado, M.P. Stability, lubricity, viscosity, and cold-flow properties of alcohol-diesel blends. *Energy Fuels* **2010**, *24*, 4497–4502. [[CrossRef](#)]
25. Ren, Y.; Huang, Z.; Miao, H.; Di, Y.; Jiang, D.; Zeng, K.; Liu, B.; Wang, X. Combustion and emissions of a DI diesel engine fuelled with diesel-oxygenate blends. *Fuel* **2008**, *87*, 2691–2697. [[CrossRef](#)]

26. Li, T.; Ogawa, H. Analysis of the trade-off between soot and nitrogen oxides in diesel-like combustion by chemical kinetic calculation. *SAE Int. J. Engines* **2011**, *5*, 94–101. [[CrossRef](#)]
27. Chang, Y.-C.; Lee, W.-J.; Wu, T.S.; Wu, C.-Y.; Chen, S.-J. Use of water containing acetone–butanol–ethanol for NO_x-PM (nitrogen oxide-particulate matter) trade-off in the diesel engine fueled with biodiesel. *Energy* **2014**, *64*, 678–687. [[CrossRef](#)]
28. Asad, U.; Kumar, R.; Zheng, M.; Tjong, J. Ethanol-fueled low temperature combustion: a pathway to clean and efficient diesel engine cycles. *Appl. Energy* **2015**, *157*, 838–850. [[CrossRef](#)]
29. Fang, Q.; Fang, J.; Zhuang, J.; Huang, Z. Effects of ethanol–diesel–biodiesel blends on combustion and emissions in premixed low temperature combustion. *Appl. Therm. Eng.* **2013**, *54*, 541–548. [[CrossRef](#)]
30. Jung, Y.; Park, S.S.; Bae, C. Effect of oxygen concentration on highly diluted charge compression ignition combustion in an optical engine. *Appl. Therm. Eng.* **2015**, *90*, 538–550. [[CrossRef](#)]
31. Zhou, N.; Huo, M.; Wu, H.; Nithyanandan, K.; Chia-fon, F.L.; Wang, Q. Low temperature spray combustion of acetone–butanol–ethanol (ABE) and diesel blends. *Appl. Energy* **2014**, *117*, 104–115. [[CrossRef](#)]
32. Zhao, H.; Ladommatos, N. Optical diagnostics for soot and temperature measurement in diesel engines. *Prog. Energy Combust. Sci.* **1998**, *24*, 221–255. [[CrossRef](#)]
33. Jing, W.; Wu, Z.; Zhang, W.; Fang, T. Measurements of soot temperature and KL factor for spray combustion of biomass derived renewable fuels. *Energy* **2015**, *91*, 758–771. [[CrossRef](#)]
34. Zhang, J.; Jing, W.; Roberts, W.L.; Fang, T. Soot temperature and KL factor for biodiesel and diesel spray combustion in a constant volume combustion chamber. *Appl. Energy* **2013**, *107*, 52–65. [[CrossRef](#)]
35. Matsui, Y.; Kamimoto, T.; Matsuoka, S. *A Study on the Time and Space Resolved Measurement of Flame Temperature and Soot Concentration in a DI Diesel Engine by the Two-Color Method*; SAE Technical Paper 0148-7191; Society of Automotive Engineers: Melbourne, Australia, 1979.
36. Shi, Q.; Li, T.; Zhang, X.; Wang, B.; Zheng, M. *Measurement of Temperature and Soot (KL) Distributions in Spray Flames of Diesel-Butanol Blends by Two-Color Method Using High-Speed RGB Video Camera*; SAE Technical Paper 0148-7191; Society of Automotive Engineers: Baltimore, MD, USA, 2016.
37. Ma, H.; Stevens, R.; Stone, R. *In-Cylinder Temperature Estimation from an Optical Spray-Guided DISI Engine with Color-Ratio Pyrometry (CRP)*; SAE Technical Paper 0148-7191; Society of Automotive Engineers: Detroit, MI, USA, 2006.
38. Shah, R.K.; Shum, H.C.; Rowat, A.C.; Lee, D.; Agresti, J.J.; Utada, A.S.; Chu, L.; Kim, J.; Fernandeznieves, A.; Martinez, C.J. Designer emulsions using microfluidics. *Mater. Today* **2008**, *11*, 18–27. [[CrossRef](#)]
39. Hiroyasu, H.; Kadota, T.; Arai, M. Supplementary comments: fuel spray characterization in diesel engines. *Combust. Model. Recipr. Engines* **1980**, *369*, 309–321.
40. Kiplimo, R.; Tomita, E.; Kawahara, N.; Yokobe, S. Effects of spray impingement, injection parameters, and EGR on the combustion and emission characteristics of a PCCI diesel engine. *Appl. Therm. Eng.* **2012**, *37*, 165–175. [[CrossRef](#)]
41. Lahane, S.; Subramanian, K.A. Impact of nozzle holes configuration on fuel spray, wall impingement and NO_x emission of a diesel engine for biodiesel–diesel blend (B20). *Appl. Therm. Eng.* **2014**, *64*, 307–314. [[CrossRef](#)]
42. Mueller, C.J.; Boehman, A.L.; Martin, G.C. An experimental investigation of the origin of increased NO_x emissions when fueling a heavy-duty compression-ignition engine with soy biodiesel. *SAE Int. J. Fuels Lubr.* **2009**, *2*, 789–816. [[CrossRef](#)]
43. Pickett, L.M.; Siebers, D.L. Soot in diesel fuel jets: Effects of ambient temperature, ambient density, and injection pressure. *Combust. Flame* **2004**, *138*, 114–135. [[CrossRef](#)]
44. Tree, D.R.; Svensson, K.I. Soot processes in compression ignition engines. *Prog. Energy Combust. Sci.* **2007**, *33*, 272–309. [[CrossRef](#)]
45. López, J.J.; Martín, J.; García, A.; Villalta, D.; Warey, A. Implementation of two color method to investigate late cycle soot oxidation process in a CI engine under low load conditions. *Appl. Therm. Eng.* **2017**, *113*, 878–890. [[CrossRef](#)]

